THE JOURNAL OF PHYSICAL CHEMISTRY LETTERS
A JOURNAL OF THE AMERICAN CHEMICAL SOCIETY

pubs.acs.org/JPCL

Letter

Morphogenesis in Synthetic Chemical Cells

Leonardo Silva-Dias* and Alejandro Lopez-Castillo*

Cite This: J. Phys. Chem. Lett. 2022, 13, 296−301

Read Online

ACCESS | Metrics & More | Article Recommendations | Supporting Information

ABSTRACT: We present an efficient model for describing morphogenesis and the emergence of spatiotemporal structures in synthetic chemical cells. This work is motivated by an experimental setup used for testing Turing's theory of morphogenesis. The model developed is based on the general theory of chemically active droplets, which combines the classical theory of phase separation with reaction-diffusion systems. Through the 2D calculations, we find the six spatiotemporal structures predicted by Turing in 1952 and experimentally observed, in a 1D array of droplets. Moreover, under Turing instability, with a determined chemical wavelength, the system undergoes morphogenesis. This theoretical approach provides a useful tool for understanding the physical differentiation through the direct calculation of the osmotic pressure in each cell as the chemical reaction occurs.

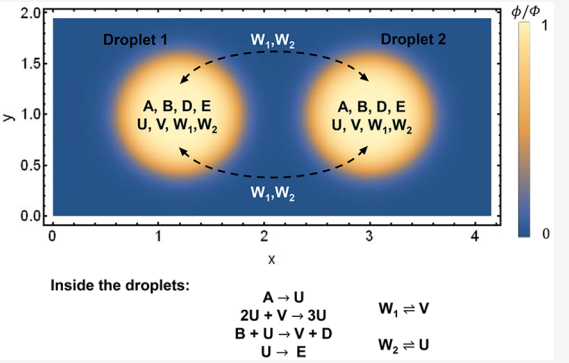

In a broad sense, morphogenesis is the generation of patterns and shapes, induced by the dynamical interplay between chemical and physical processes.[1] The earliest theoretical description of such an event was proposed by Alan M. Turing in his seminal 1952 article "The chemical basis of morphogenesis".[2] In this paper, Turing presents a model that is applicable for two cases: (1) a homogeneous ring of continuous material and (2) a heterogeneous ring of discrete compartments, i.e., cells.[2−4] The second case is more relevant in biology because such a configuration arises naturally during the developmental process.[3] However, the Turing model cannot be used for making predictions in this context due to the difficulties of comparison of experiment and theory.[3,5] To overcome this problem, Tompkins et al. reported an experimental reaction−diffusion system for testing Turing's theory of morphogenesis.[3] Such a system is formed by synthetic "cells", i.e., aqueous droplets containing the Belousov−Zhabotinsky (BZ) chemical reactants, stabilized by surfactant in dispersed oil. The main point in such a construction is that most of the chemical species in the BZ reaction are polar, remaining trapped in the cells. However, less-polar intermediates are also formed, and they can diffuse through the oil medium, acting as chemical signals.[3,6,7] Technically, it represents an array of chemical oscillators coupled by diffusion. From this experiment, Tompkins et al. confirmed Turing's theory, reporting the emergence of the seven spatiotemporal structures (six of them predicted by Turing and one not) and the physical differentiation of cells under Turing instability.

Considering the experimental setup exposed previously and the general theory of chemically active droplets, we present in this letter a continuous heterogeneous model for describing morphogenesis and the emergence of spatiotemporal structures in synthetic chemical cells. Unlike earlier dynamical models, here we use the classical theory of phase separation to explicitly take into account the dynamics of chemical cells.[3,6−13] From that, we can study the effects of chemical reactions on the droplets; we also can vary the droplet radius, the droplet−droplet distance, and the spatial arrangement of the droplets (1D and 2D). Thus, this model provides a new means of theoretically describing coupled chemical oscillators and exploring the physical-chemical properties of such systems. We show morphogenesis in this heterogeneous reaction−diffusion system happens through a well-defined chemical−physical mechanism.

We consider a system composed of an incompressible, isothermal fluid with constant molecular volumes (ν) containing a nonpolar (N) component, which forms the background fluid, and a polar (P) component, which forms droplets by phase separation. We denote the local volume fraction of the P component by $\phi(\mathbf{r}, t)$, and from the incompressibility condition we can determine the local volume fraction of the N component in terms of ϕ. Therefore, the phase separation dynamics are given by the Cahn−Hilliard equation[9,14,15]

$$\frac{\partial \phi}{\partial t} = s(\mathbf{c}) + m\nabla^2 \frac{\delta F[\phi]}{\delta \phi} \tag{1}$$

Received: November 1, 2021
Accepted: December 27, 2021
Published: January 6, 2022

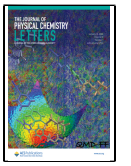

https://doi.org/10.1021/acs.jpclett.1c03573
J. Phys. Chem. Lett. 2022, 13, 296−301

In eq 1 m is the mobility coefficient of the droplet material, $s(\mathbf{c})$ represents the local homogeneous reaction processes and obeys the laws of chemical kinetics, and $F[\phi]$ is the free energy given by the Ginzburg–Landau functional,[9]

$$F[\phi] = \int \mathrm{d}^2 r \left[-\frac{\beta}{2}(\phi - \psi)^2 + \frac{\alpha}{4}(\phi - \psi)^4 + \frac{\kappa}{2}|\nabla\phi|^2 \right] \tag{2}$$

In this equation, the positive parameters α and β are related to the energetic interactions and entropic contributions, and the coefficient κ is associated with the surface tension and the interface width. Moreover, the double-well potential $f(\phi)$, i.e., $f(\phi) = -\frac{\beta}{2}(\phi - \psi)^2 + \frac{\alpha}{4}(\phi - \psi)^4$, in eq 2 accounts for the separation of the fluid in two phases: an N-rich phase, $\phi = 0$, and a P-rich phase, $\phi = \Phi$. From that, we use $\psi = \Phi/2$.[10,11]

We can describe arrays of polar droplets from eq 1, considering the following *ansatz* for the initial condition:

$$\phi(\mathbf{r}, 0) = \frac{\Phi}{2}\left[1 - \prod_i^M \tanh\left(\frac{d_i}{\omega}\right)\right] \tag{3}$$

In eq 3, M is the number of droplets, $d_i = \sqrt{(x - x_i^*)^2 + (y - y_i^*)^2} - R$, (x_i^*, y_i^*) are the coordinates of the center of the ith droplet, R is the droplet radius, and $\omega = \sqrt{\frac{2\kappa}{\beta}}$ is the interface width. Equation 3 is based on the spatial profile of the volume fraction that minimizes the free energy $F[\phi]$, considering a system with a flat interface between two phases with $\phi = 0$ and $\phi = \Phi$ in the bulk.[10]

We highlight that the resultant arrangement of droplets is dynamically unstable. However, it can be maintained "stable" if we ideally avoid numerical and physical fluctuations on the system and keep the droplets sufficiently apart from each other. This fact can be realized from the Lifshitz–Slyozov model.[16] Such a model demonstrates that in a finite system an isolated droplet has a stationary state.[11] Therefore, we can combine copies of isolated droplets ensuring they do not undergo Ostwald ripening. With that, we can neglect surfactants in the description of our theoretical approach, even though they are used in the experiment.

Now, we must specify the reaction mechanism and the dynamical equations of its chemical components. After that, we are going to be able to define $s(\mathbf{c})$. In this work, we use the generic "extended Brusselator" model.[17,18] This system is written as

$$\mathrm{A} \xrightarrow{k_1} \mathrm{U}$$

$$2\mathrm{U} + \mathrm{V} \xrightarrow{k_2} 3\mathrm{U}$$

$$\mathrm{B} + \mathrm{U} \xrightarrow{k_3} \mathrm{V} + \mathrm{D}$$

$$\mathrm{U} \xrightarrow{k_4} \mathrm{E}$$

$$\mathrm{V} \underset{d_1}{\overset{c_1}{\rightleftharpoons}} \mathrm{W}_1$$

$$\mathrm{U} \underset{d_2}{\overset{c_2}{\rightleftharpoons}} \mathrm{W}_2$$

where U and V are the polar activator and inhibitor species, W_1 and W_2 are the less-polar chemical signals, A and B are polar constant reactants responsible for maintaining the system far from equilibrium, and E and D are the polar products. From the features of the chemicals, U, V, A, B, D, and E are kept arrested inside the droplets, whereas W_1 and W_2 can freely diffuse through the entire system. Despite such a reaction being abstract, it satisfies basic requirements for activator–inhibitor systems; i.e., it has positive and negative feedbacks, enabling the study of coupled chemical oscillators.[18]

Following the law of mass action, we can write the spatiotemporal dynamic equations as

$$\frac{\partial u}{\partial t} = f(u, v) - c_2 u + d_2 w_2 + \left(D_u^{(P)} \frac{\phi}{\Phi} + D_u^{(N)} \left(1 - \frac{\phi}{\Phi}\right)\right)\nabla^2 u \tag{4}$$

$$\frac{\partial v}{\partial t} = g(u, v) - c_1 v + d_1 w_1 + \left(D_v^{(P)} \frac{\phi}{\Phi} + D_v^{(N)} \left(1 - \frac{\phi}{\Phi}\right)\right)\nabla^2 v \tag{5}$$

$$\frac{\partial w_1}{\partial t} = (c_1 v - d_1 w_1)\Theta(r) + \left(D_{w_1}^{(P)} \frac{\phi}{\Phi} + D_{w_1}^{(N)} \left(1 - \frac{\phi}{\Phi}\right)\right)\nabla^2 w_1 \tag{6}$$

$$\frac{\partial w_2}{\partial t} = (c_2 u - d_2 w_2)\Theta(r) + \left(D_{w_2}^{(P)} \frac{\phi}{\Phi} + D_{w_2}^{(N)} \left(1 - \frac{\phi}{\Phi}\right)\right)\nabla^2 w_2 \tag{7}$$

In these equations, u, v, w_1, and w_2 are the chemical concentrations of U, V, W_1, and W_2, respectively. They all are defined through the system's total volume. The diffusion coefficients in the polar and nonpolar phases are $D^{(P)}$ and $D^{(N)}$, respectively, and k_1, k_2, k_3, k_4, c_1, d_1, c_2, and d_2 are the kinetic rate constants. Furthermore, the Brusselator kinetics are given by $f(u, v) = k_1 a - (k_4 + k_3 b)u + k_2 u^2 v$ and $g(u, v) = k_3 b u - k_2 u^2 v$, with a and b the chemical concentrations of A and B, respectively.

We can realize eqs 4–7 are coupled to the phase dynamics through the mass transport process, resulting in a spatially dependent diffusion coefficient. Therefore, taking $D_u^{(P)} = D_v^{(P)} \neq 0$, $D_u^{(N)} = D_v^{(N)} = 0$, and $D_{w_1}^{(P)} = D_{w_2}^{(P)} < D_{w_1}^{(N)} = D_{w_2}^{(N)} \neq 0$, relations experimentally measured, we can guarantee that U and V only diffuse inside the cells and W_1 and W_2 can diffuse in both phases, although with different diffusion coefficients in each one of them.[3,6−8,19−21] Note, as well, that in eqs 6 and 7, we added an *ad hoc* Heaviside step function, $\Theta(r)$, for ensuring chemical reactions only happen inside the cells, as is experimentally observed. See in the Supporting Information I about the coupling among the reaction–diffusion and phase separations equations, and the definition of $\Theta(r)$.

To complete our model construction, we now define $s(\mathbf{c})$. This term describes the effects of chemical reactions on the dynamics of phase separation, in a way that if $s(\mathbf{c}) = 0$, morphogenesis cannot emerge. The kinetic terms of the phase separation equation are derived assuming such a phase is composed of solvent and chemical volume fractions, resulting in the final phase separation:

$$\frac{\partial \phi}{\partial t} = \eta k(-a + u) + m\nabla^2 \frac{\delta F[\phi]}{\delta \phi} \tag{8}$$

In eq 8, k is the reaction rate constantl in this work we use $k_1 = k_2 = k_3 = k_4 = k$. η is a constant that represents the dilution of chemicals in the P-phase. See a detailed derivation of eq 8 in the Supporting Information II.

https://doi.org/10.1021/acs.jpclett.1c03573
J. Phys. Chem. Lett. 2022, 13, 296−301

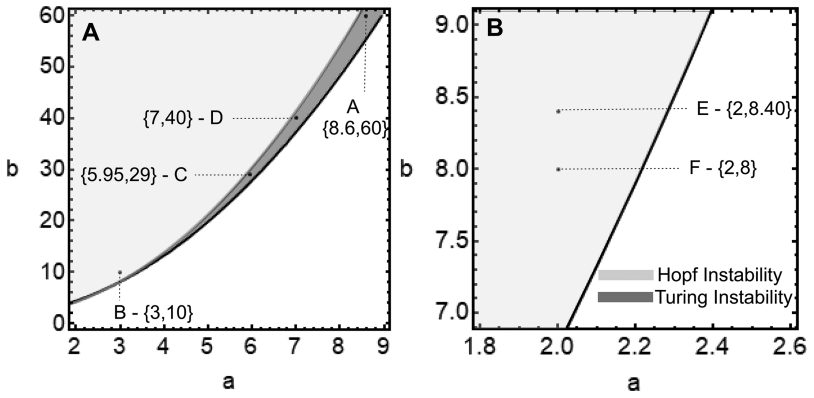

Figure 1. For both parameter spaces $k_1 = k_2 = k_3 = k_4 = k = 0.07$, $D_u^{(P)} = D_v^{(P)} = 10^{-3}$, $D_u^{(N)} = D_v^{(N)} = 0.0$, $D_{w_1}^{(P)} = D_{w_2}^{(P)} = 10^{-2}$, and $D_{w_1}^{(N)} = D_{w_2}^{(N)} = 5.5 \times 10^{-2}$. (A) Parameter space $(a \times b)$ of the model highly coupled to the inhibitor with $c_1 = 0.14$, $d_1 = 0.35$, $c_2 = d_2 = 7 \times 10^{-3}$. (B) Parameter space $(a \times b)$ of the model highly coupled to the activator with $c_2 = 0.14$, $d_2 = 0.35$, $c_1 = d_1 = 7 \times 10^{-3}$. The pairs (a, b) indicated are used in the numerical simulations in Figure 2A–F.

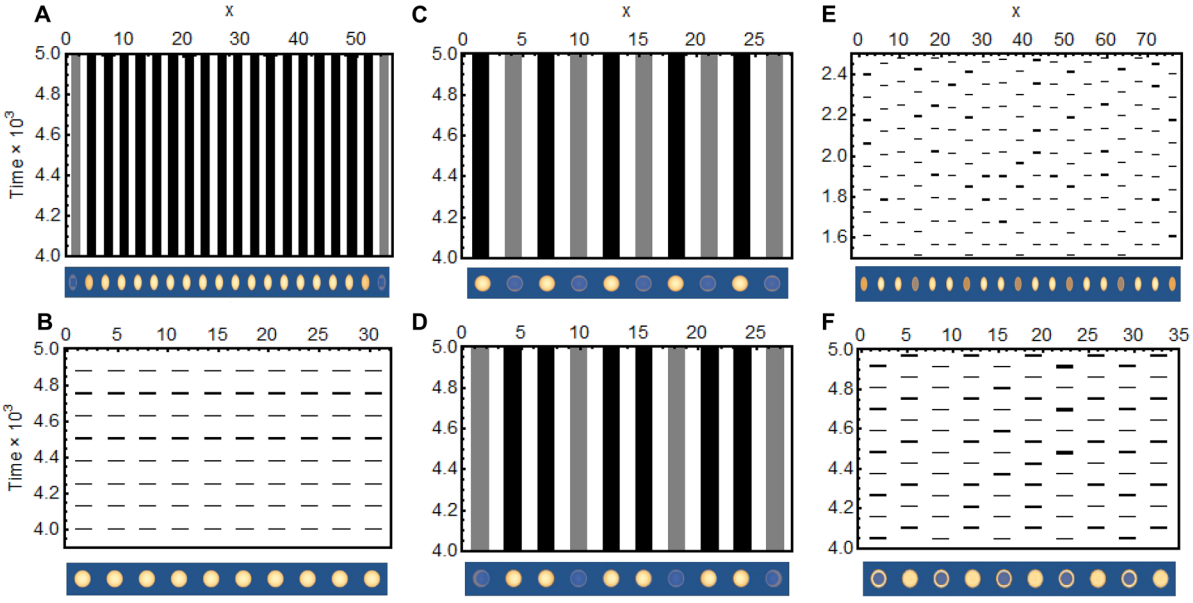

Figure 2. Space–time plots exposing the six cases predicted by Turing. At the base of each plot, there is the spatial profile of the inhibitor at a specific time. These numerical simulations were carried out considering the parameters presented in Figure 1A,B, $\Phi = 2$, $m = 10^{-3}$, $\alpha = \beta = 6.66$, and $\kappa = 0.133$. (A) Long-wavelength and stationary $(q_{min}, 0)$, 20 cells with radius $R = 0.70$, oil gap $d = 2R$, and the spatial profile of v taken at $t = 4500$. (B) Long-wavelength and oscillatory (q_{min}, ω), 10 cells with radius $R = 0.80$, oil gap $d = 2R$, and the spatial profile of v taken at $t = 4200$. (C) Short-wavelength and stationary $(q_{max}, 0)$, 10 cells with radius $R = 0.70$, oil gap $d = 2R$, and the spatial profile of v taken at $t = 4000$. (D) Intermediate-wavelength and stationary $(q, 0)$, 10 cells with radius $R = 0.70$, oil gap $d = 2R$, and the spatial profile of v taken at $t = 4000$. (E) Intermediate-wavelength and oscillatory (q, ω), 19 cells with radius $R = 0.82$, oil gap $d = 3R$, and the spatial profile of v taken at $t = 2400$. (F) Short-wavelength and oscillatory (q_{max}, ω), 10 cells with radius $R = 0.86$, oil gap $d = 2R$, and the spatial profile of v taken at $t = 4050$.

Together, eqs 4, 5, 6, 7, and 8 represent the model for describing morphogenesis in synthetic chemical cells. These equations are numerically solved using the xmds2 software package (version 2.2.2) with an adaptive fourth–fifth order Runge–Kutta and spectral methods for computing the spatial derivatives.[22] The simulations are carried out in two-dimensional rectangular lattices, with periodic boundary conditions.

We are initially interested in the situation where the volume fraction of the chemicals is much lower than the solvent's volume fraction, i.e., when $\eta \approx 0$. It means that the chemical reactions do not affect the dynamics of phase separation. Through this approach, we focus on the emergence of spatiotemporal chemical structures; more specifically, we seek those structures predicted by Turing and experimentally observed by Tompkins et al. To accomplish that, we perform a stability analysis of the homogeneous linear version of eqs 4–7 to define the right parameters for Turing and Hopf instability. See such a treatment in the Supporting Information III.

Figure 1A,B shows the parameter spaces $(a \times b)$ of the model with chemical signals highly coupled through the inhibitor and the activator, respectively. The parameters used to perform such an analysis are based on experimental and theoretical data reported in the literature.[3,6−9,19−21] As it is expected, the first case satisfies the long-range inhibition and short-range excitation condition needed for the Turing instability, favoring the emergence of stationary patterns. Whereas, in the second case, the excitation-inhibition range conditions are not fulfilled, so the Hopf dynamics prevail.

https://doi.org/10.1021/acs.jpclett.1c03573
J. Phys. Chem. Lett. 2022, 13, 296−301

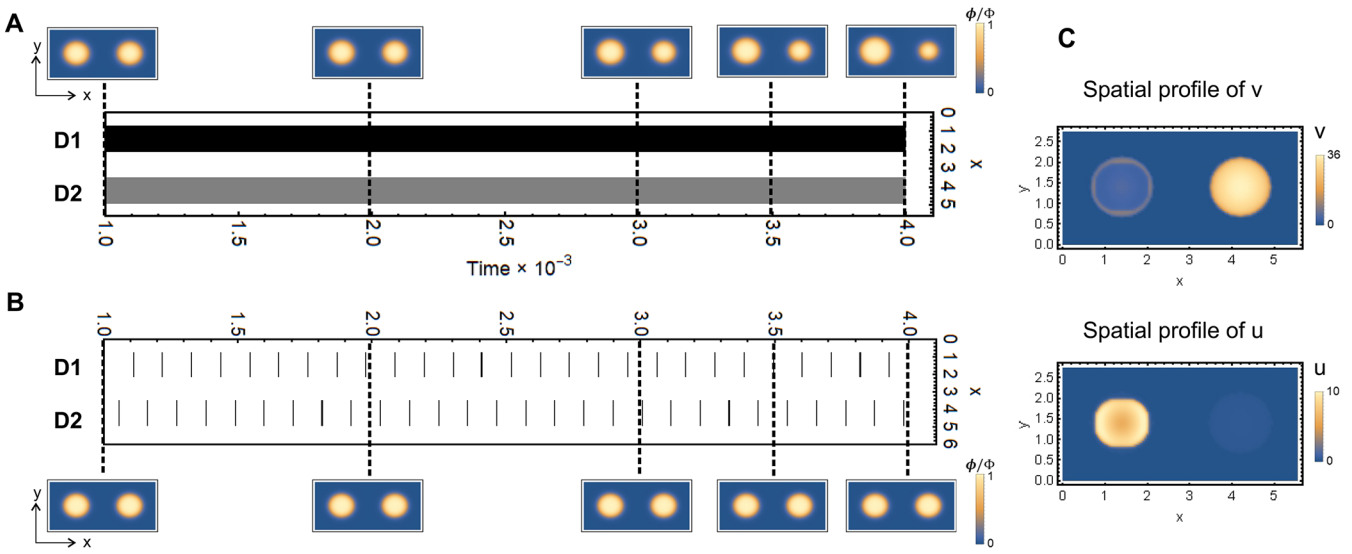

Figure 3. In all simulations we used $\eta = 10^{-4}$. (A) Space−time plot of the short-wavelength stationary pattern of the system composed of droplet 1 (D1) and droplet 2 (D2). The black dashed lines indicate the time that the spatial profiles of the phase ϕ, above, are taken. (B) Space−time plot of the short-wavelength oscillatory pattern of the system composed of droplet 1 (D1) and droplet 2 (D2). The black dashed lines indicate the time that the spatial profiles of the phase ϕ, below, are taken. (C) Spatial profiles of the inhibitor, v, and activator, u, at $t = 2000$ in the system under Turing instability.

Considering the parameters indicated in Figure 1A,B in the numerical simulations, we could obtain the six spatiotemporal chemical structures, in a 1D array of cells, presented in Figure 2A−F. Each one of these chemical states is classified following Turing's notation, i.e., in terms of wavelength and frequency. Such dynamical states have a crucial dependence on the cells' radius and the gaps, between the cells, in a way that stationary patterns are favored in systems with smaller cells and gaps, whereas oscillatory patterns are favored in systems with larger cells and gaps. Another interesting aspect is that out-of-phase and in-phase oscillations only appear in the cases that chemical signals are highly coupled to activator and inhibitor, respectively. These relations mentioned are in agreement with experimental and theoretical investigations previously reported.[3,8,18]

Once we have found the stationary and oscillatory patterns from the numerical simulations, we now focus on morphogenesis, i.e., the morphological change of the chemical cell activated by chemical reactions. Here, the physical processes, i.e., the phase separation, are regulated by the chemical reactions. Therefore, $\eta \neq 0$. In this case, we study shape variations in a system composed of two cells, when (1) a short-wavelength stationary pattern and (2) a short-wavelength oscillatory pattern emerge. See the results in Figure 3A,B, as well as, in Movies S1 and S2 in the Supporting Information.

In case (1), the simulation reveals that as the chemical reaction evolves over time the chemical cells suffer physical differentiation, i.e., the droplet 1 (D1) swells and the droplet 2 (D2) shrinks, see Figure 3A and Movie S1, in the Supporting Information. To understand the mechanism of this event, we calculate the temporal evolution of the osmotic pressure (Π), given by $\Pi = -f(\phi) + \frac{\partial f(\phi)}{\partial \phi}$, in each cell.[9] We see from the spatial profile of the activator and inhibitor species, Figure 3C, that the Turing dynamical state is marked by the asymmetrical consumption and formation of reactants and products, respectively, between the cells. As a consequence, the internal concentration of chemicals in D1 becomes greater than in D2, creating an osmotic pressure imbalance, as is shown in Figure 4A. Such an imbalance in the osmotic pressure induces flows of

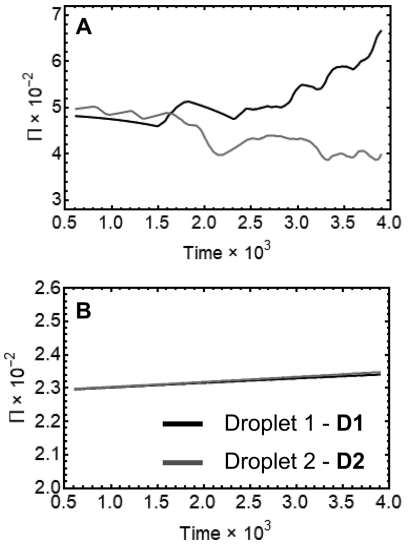

Figure 4. Temporal evolution of the moving average of the osmotic pressure (Π). The moving average is calculated over the last 30 points of the osmotic pressure to generate a smoothed curve. (A) Stationary pattern with short wavelength. (B) Oscillatory pattern with short wavelength.

solvent from D2 to D1, causing the swelling of this cell to the detriment of the shrinking of the other one. Therefore, morphogenesis in synthetic chemical cells follows this well-established chemical−physical mechanism described above.

Note that, differently from what was observed experimentally, the morphogenetic process described by this model proceeds until the droplet with lower osmotic pressure completely disappears. It happens because the shape variations caused by morphogenesis triggers Ostwald ripening. Such a phenomenon cannot be controlled due to the lack of surfactant on the model, as we have argued. Therefore, to avoid any confusion, it is reasonable to distinguish each phenomenon, i.e., morphogenesis and Ostwald ripening. To do so, we perform two simulations of the same system with (I) $\eta = 0$ and $R_1^0 = R_2^0$ and (II) $\eta = 0$, $R_1^0 = R$

https://doi.org/10.1021/acs.jpclett.1c03573
J. Phys. Chem. Lett. 2022, 13, 296−301

$+\delta$, $R_2^0 = R$, where $R_{1,2}^0$ are the initial radii of D1 and D2. Through these simulations we can realize the main differences between the processes; see the Supporting Information IV.

In case (2), the results show chemical cells do not physically differentiate; see Figure 3B and Movie S2 in the Supporting Information. In this situation, the activator−inhibitor dynamics are characterized by out-of-phase oscillation. Such a state momentarily creates differences in the internal concentration of the droplets; however, they are reversible due to the periodic behavior of the chemical reaction. In these conditions, the osmotic pressure presents some small variations, Figure 4B, but these variations are neither large enough nor kept long enough to activate physical morphogenesis.

In this letter, we have theoretically studied morphogenesis and the emergence of spatiotemporal structures in synthetic chemical cells. We have found the six spatiotemporal chemical structures predicted by Turing and experimentally observed by Tompkins et al. We have verified a strong dependence between these structures and the geometrical features of the arrangement of the cells, such as Turing and Hopf states emerging on a system formed by smaller and greater radii and gaps, respectively. Moreover, the out-of-phase oscillations are favored in a system where the chemical signals are highly coupled to the activator, whereas the in-phase oscillations are favored in a system where the chemical signals are highly coupled to the inhibitor.

We have precisely shown that morphogenesis of these nonbiological cells follows a well-defined sequence of events: (1) emergence of Turing patterns creating local asymmetries of the chemical processes, i.e., chemical differentiation, (2) propagation of a significant difference of the osmotic pressure between the synthetic cells, (3) generation of flows of solvent from the cell with lower osmotic pressure to the cell of higher osmotic pressure, and (4) shape variation, i.e., physical morphogenesis. Under Hopf instability, the chemical cells do not physically differentiate; once in this state, no local chemical asymmetries emerge.

We have demonstrated that the model proposed in this work is sufficient to describe all the main phenomena reported by Tompkins et al. in the experiment used for testing Turing's theory of morphogenesis. It also offers a simple way to theoretically describe complex 1D and 2D arrays of chemical oscillators coupled by diffusion. In conclusion, this model is a useful tool for designing new experiments of heterogeneous reaction−diffusion systems, exploring dynamical states still not observed in such arrangements, and understanding physical phenomena, as shape variations.

■ ASSOCIATED CONTENT

Supporting Information

The Supporting Information is available free of charge at https://pubs.acs.org/doi/10.1021/acs.jpclett.1c03573.

Detailed deductions, linear stability analysis, and extra simulations (PDF)

Spatial profile of the phase ϕ and time evolution of the activator, U, and inhibitor, V, at the center of the cells in the system under Turing instability (MP4)

Spatial profile of the phase ϕ and time evolution of the activator, U, at the center of the cells in the system under Hopf instability (MP4)

■ AUTHOR INFORMATION

Corresponding Authors

Leonardo Silva-Dias − *Chemistry Department, Federal University of São Carlos, São Carlos, São Paulo 13 565-905, Brazil*; orcid.org/0000-0003-0535-6666; Email: leonardosilvadias@estudante.ufscar.br

Alejandro Lopez-Castillo − *Chemistry Department, Federal University of São Carlos, São Carlos, São Paulo 13 565-905, Brazil*; Email: alcastil@ufscar.br

Complete contact information is available at: https://pubs.acs.org/10.1021/acs.jpclett.1c03573

Notes

The authors declare no competing financial interest.

■ ACKNOWLEDGMENTS

This work was financially supported by the São Paulo Research Foundation (FAPESP), Grants 2019/12501-0 and 2019/23205-3, and Coordenação de Aperfeicoamento de Pessoal de Nível Superior (CAPES), finance code 001. The authors thank Dr. Raphael Nagao and the referees for their helpful comments. The authors are also grateful to the HPC resources provided by the SDumont supercomputer at the National Laboratory for Scientific Computing (LNCC/MCTI, Brazil) and by the Cluster - UFSCar.

■ REFERENCES

(1) Mietke, A.; Jülicher, F.; Sbalzarini, I. F. Self-organized shape dynamics of active surfaces. *Proc. Natl. Acad. Sci. U. S. A.* **2019**, *116*, 29−34.

(2) Turing, A. M. The chemical basis of morphogenesis. *Phylosophical Transactions of the Royal Society of London* **1952**, *237*, 37−72.

(3) Tompkins, N.; Li, N.; Girabawe, C.; Heymann, M.; Ermentrout, G. B.; Epstein, I. R.; Fraden, S. Testing Turing's theory of morphogenesis in chemical cells. *Proc. Natl. Acad. Sci. U. S. A.* **2014**, *111*, 4397−4402.

(4) Silva-Dias, L.; Lopez-Castillo, A. Turing patterns modulation by chemical gradient in isothermal and non-isothermal conditions. *Phys. Chem. Chem. Phys.* **2020**, *22*, 7507−7515.

(5) Reinitz, J. Pattern formation. *Nature* **2012**, *482*, 464−464.

(6) Delgado, J.; Li, N.; Leda, M.; González-Ochoa, H. O.; Fraden, S.; Epstein, I. R. Coupled oscillations in a 1D emulsion of Belousov−Zhabotinsky droplets. *Soft Matter* **2011**, *7*, 3155−3167.

(7) Toiya, M.; Vanag, V. K.; Epstein, I. R. Diffusively coupled chemical oscillators in a microfluidic assembly. *Angew. Chem.* **2008**, *120*, 7867−7869.

(8) Toiya, M.; González-Ochoa, H. O.; Vanag, V. K.; Fraden, S.; Epstein, I. R. Synchronization of chemical micro-oscillators. *J. Phys. Chem. Lett.* **2010**, *1*, 1241−1246.

(9) Weber, C. A.; Zwicker, D.; Jülicher, F.; Lee, C. F. Physics of active emulsions. *Rep. Prog. Phys.* **2019**, *82*, 064601.

(10) Zwicker, D.; Seyboldt, R.; Weber, C. A.; Hyman, A. A.; Jülicher, F. Growth and division of active droplets provides a model for protocells. *Nat. Phys.* **2017**, *13*, 408−413.

(11) Zwicker, D.; Hyman, A. A.; Jülicher, F. Suppression of Ostwald ripening in active emulsions. *Phys. Rev. E* **2015**, *92*, 012317.

(12) Zwicker, D.; Baumgart, J.; Redemann, S.; Müller-Reichert, T.; Hyman, A. A.; Jülicher, F. Positioning of particles in active droplets. *Physical review letters* **2018**, *121*, 158102.

(13) Lee, C. F.; Brangwynne, C. P.; Gharakhani, J.; Hyman, A. A.; Jülicher, F. Spatial organization of the cell cytoplasm by position-dependent phase separation. *Physical review letters* **2013**, *111*, 088101.

(14) Cahn, J. W.; Hilliard, J. E. Free energy of a nonuniform system. I. Interfacial free energy. *J. Chem. Phys.* **1958**, *28*, 258−267.

(15) Cahn, J. W. On spinodal decomposition. *Acta Metall.* **1961**, *9*, 795−801.
(16) Lifshitz, I. M.; Slyozov, V. V. The kinetics of precipitation from supersaturated solid solutions. *Journal of physics and chemistry of solids* **1961**, *19*, 35−50.
(17) Nicolis, G.; Prigogine, I. *Self-Organisation in Nonequilibrium Systems*; Wiley: New York, 1977.
(18) Vanag, V. K.; Epstein, I. R. Diffusive instabilities in heterogeneous systems. *J. Chem. Phys.* **2003**, *119*, 7297−7307.
(19) Vanag, V. K.; Epstein, I. R. Pattern formation in a tunable medium: The Belousov-Zhabotinsky reaction in an aerosol OT microemulsion. *Physical review letters* **2001**, *87*, 228301.
(20) Vanag, V. K.; Epstein, I. R. Stationary and oscillatory localized patterns, and subcritical bifurcations. *Physical review letters* **2004**, *92*, 128301.
(21) Vanag, V. K.; Epstein, I. R. A model for jumping and bubble waves in the Belousov−Zhabotinsky-aerosol OT system. *J. Chem. Phys.* **2009**, *131*, 104512.
(22) Dennis, G. R.; Hope, J. J.; Johnsson, M. T. XMDS2: Fast, scalable simulation of coupled stochastic partial differential equations. *Comput. Phys. Commun.* **2013**, *184*, 201−208.

https://doi.org/10.1021/acs.jpclett.1c03573
J. Phys. Chem. Lett. 2022, 13, 296−301